Imaging biomarkers of lung ventilation in interstitial lung disease from 129Xe and oxygen enhanced 1H MRI

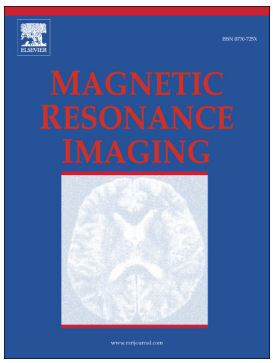

Imaging biomarkers of lung ventilation in interstitial lung disease from 129Xe and oxygen enhanced 1H MRI

Marta Tibiletti, James A. Eaden, Jo Naish, Paul J.C. Hughes, John C. Waterton, Matthew J. Heaton, Nazia Chaudhuri, Sarah Skeoch, Ian N. Bruce, Stephen Bianchi, Jim M. Wild, Geoff J.M. Parker

PII: S0730-725X(22)00177-1

DOI: https://doi.org/10.1016/j.mri.2022.10.005

Reference: MRI 9873

To appear in: *Magnetic Resonance Imaging*

Received date: 18 May 2022

Revised date: 7 October 2022

Accepted date: 11 October 2022

Please cite this article as: M. Tibiletti, J.A. Eaden, J. Naish, et al., Imaging biomarkers of lung ventilation in interstitial lung disease from 129Xe and oxygen enhanced 1H MRI, *Magnetic Resonance Imaging* (2022), https://doi.org/10.1016/j.mri.2022.10.005

Imaging biomarkers of lung ventilation in Interstitial Lung Disease from ^{129}Xe and Oxygen Enhanced ^{1}H MRI

Marta Tibiletti[a], James A Eaden[b], Jo Naish[a,c], Paul JC Hughes[b], John C Waterton[a,d], Matthew J Heaton[a], Nazia Chaudhuri[e], Sarah Skeoch[f], Ian N Bruce[g,h], Stephen Bianchi[i], Jim M Wild[b,j], Geoff JM Parker[a,k]

a: Bioxydyn Limited, Rutherford House, Manchester Science Park, Manchester, M15 6SZ, United Kingdom

b: POLARIS, University of Sheffield MRI unit, Department of Infection, Immunity and Cardiovascular Disease, The University of Sheffield, Sheffield, UK

c: MCMR, Manchester University NHS Foundation Trust, Wythenshawe, Manchester, UK

d: Centre for Imaging Sciences, University of Manchester, Manchester, UK

e: North West Lung Centre, Manchester University NHS Foundation Trust, Manchester Academic Health Science Centre, Manchester, UK

f: Royal National Hospital for Rheumatic Diseases, Royal United Hospitals Bath NHS Foundation Trust, Bath, UK

g: NIHR Manchester Biomedical Research Centre, Manchester University Hospitals NHS Foundation Trust, Manchester, UK

h: Centre for Musculoskeletal Research, University of Manchester, Manchester Academic Health Science Centre, Manchester, UK

i: Academic Directorate of Respiratory Medicine, Sheffield Teaching Hospitals NHS Foundation Trust, Sheffield, UK

j: Insigneo Insititute for in silico medicine, Sheffield, UK

k: Centre for Medical Image Computing, Department of Medical Physics and Biomedical Engineering, University College London, London, UK

Corresponding Author: Professor Geoff JM Parker, Centre for Medical Image Computing, 1st Floor 90 High Holborn, London, WC1V 6LJ; geoff.parker@ucl.ac.uk

ABSTRACT

PURPOSE: To compare imaging biomarkers from hyperpolarised ^{129}Xe ventilation MRI and dynamic oxygen-enhanced MRI (OE-MRI) with standard pulmonary function tests (PFT) in

interstitial lung disease (ILD) patients. To evaluate if biomarkers can separate ILD subtypes and detect early signs of disease resolution or progression.

STUDY TYPE: Prospective longitudinal.

POPULATION: Forty-one ILD (fourteen idiopathic pulmonary fibrosis (IPF), eleven hypersensitivity pneumonitis (HP), eleven drug-induced ILD (DI-ILD), five connective tissue disease related-ILD (CTD-ILD)) patients and ten healthy volunteers imaged at visit 1. Thirty-four ILD patients completed visit 2 (eleven IPF, eight HP, ten DIILD, five CTD-ILD) after 6 or 26 weeks.

FIELD STRENGTH/SEQUENCE: MRI performed at 1.5 T. Inversion recovery T_1 mapping, dynamic MRI acquisition with varying oxygen levels, and hyperpolarised ^{129}Xe ventilation MRI. Subjects underwent standard spirometry and gas transfer testing.

ASSESSMENT: Five ^{1}H MRI and two ^{129}Xe MRI ventilation metrics were compared with spirometry and gas transfer measurements.

STATISTICAL TEST: To evaluate differences at visit 1 among subgroups: ANOVA or Kruskal-Wallis rank tests with correction for multiple comparisons. To assess the relationships between imaging biomarkers, PFT, age and gender, at visit 1 and for the change between visit 1 and 2: Pearson correlations and multilinear regression models.

RESULTS: The global PFT tests could not distinguish ILD subtypes. Ventilated volumes were lower in ILD patients than in HVs when measured with ^{129}Xe MRI (HV 97.4 ± 2.6, CTD-ILD: 91.0 ± 4.8 p= 0.017, DI-ILD 90.1 ± 7.4 p=0.003, HP 92.6 ± 4.0 p= 0.013, IPF 88.1 ± 6.5 p<0.001), but not with OE-MRI. ^{129}Xe reported more heterogeneous ventilation in DI-ILD and IPF than in HV, and OE-MRI reported more heterogeneous ventilation in DI-ILD and IPF than in HP or CTD-ILD. The longitudinal changes reported by the imaging biomarkers did not correlate with the PFT changes between visits.

DATA CONCLUSION: Neither ^{129}Xe ventilation nor OE-MRI biomarkers investigated in this study were able to differentiate between ILD subtypes, suggesting that ventilation-only biomarkers are not indicated for this task. Limited but progressive loss of ventilated volume

as measured by ^{129}Xe-MRI may be present as the biomarker of focal disease progresses. OE-MRI biomarkers are feasible in ILD patients and do not correlate strongly with PFT. Both OE-MRI and ^{129}Xe MRI revealed more spatially heterogeneous ventilation in DI-ILD and IPF.

KEYWORDS: Hyperpolarised gas MRI, Oxygen Enhanced MRI, Lung MRI, Interstitial Lung Disease

1. INTRODUCTION

Interstitial lung diseases (ILD) constitute a heterogeneous group of conditions exhibiting inflammation and scarring of the lung parenchyma. Pathological changes are spatially heterogenous with varying degrees of acute inflammation and fibrosis. The ILDs have varying aetiologies and natural history. Typically, idiopathic pulmonary fibrosis (IPF), the most common ILD, has a chronic progressive phenotype, whereas other sub-types such as drug-induced ILD (DI-ILD) [1] and hypersensitivity pneumonitis (HP) [2] may reverse following withdrawal of the trigger. Diagnosis of ILDs remain a challenge, with a requirement for a multi-disciplinary assessment combining clinical history, immune profiling, lung physiology, computed tomography (CT), and lung biopsy [3]. It is important to accurately classify a subject's ILD subtype as this has an impact on the prognosis as well as the choice of the most effective treatment for the patient, e.g., antifibrotics in IPF [4] and immunosuppressants for other subtypes [1]. Thus, there is a need for improved biomarkers for precise diagnosis and monitoring of disease progression and treatment efficacy. Pulmonary function tests (PFTs) lack disease specificity as they measure the global function of the lungs only [5] and cannot interrogate regional change in ILD, unlike imaging biomarkers, which provide regional information [6]. Numerous observational studies have reported cohort predictors of ILD progression and/or mortality [7,8], however accurate prognosis for individual ILD patients remains a challenge. Most imaging biomarker studies in ILD have focused on IPF [9] in small numbers of subjects without independent validation [3].

Where repeated assessments are required, it is desirable to avoid ionising radiation, and risks from imaging contrast agents should be minimised. MRI biomarkers therefore are of particular interest, particularly when benign inhaled gases such as oxygen or hyperpolarised

129-xenon (^{129}Xe) are used to provide additional structural and physiological information [10–15]. Hyperpolarised ^{129}Xe MRI exploits the signal enhancement available following spin exchange optical pumping to allow for the direct visualisation of inhaled gases and ventilation at high resolution [16]. In this work, only ^{129}Xe ventilation MRI has been considered, and more complex techniques based on spectroscopy of dissolved ^{129}Xe [9,16] or diffusion-weighted MRI [15] were not included.

The technology to produce and visualise hyperpolarised gases in clinical settings is currently limited to few specialised centres [17], as hyperpolarised ^{129}Xe is categorised as an investigational medicinal product and the expense of the added equipment and personnel required limits its widespread use. For this reason, alternative methodologies to image ventilation are of interest. One candidate is oxygen enhanced MRI (OE-MRI), which exploits the effect of molecular oxygen on lung tissue water in conventional proton MRI. Pure oxygen and medical air are widely available in hospital settings, and their delivery can be reliably achieved with standard medical equipment [18].

OE-MRI permits quantification of change in concentration of dissolved oxygen in lung tissues induced by inhaling changed concentrations of O_2 [19], and has previously been deployed in other lung diseases [20,21]. OE-MRI is usually paired with a measurement of native T_1 in the parenchyma, itself a promising imaging biomarker of focal lung disease [22,23]. There is still little published information on the performance of such MR biomarkers in ILD, their temporal evolution, and correlations between the different MR biomarkers and conventional pulmonary function tests.

In this study we aimed: firstly, to compare imaging biomarkers derived from ^{1}H T_1 mapping, dynamic OE-MRI and hyperpolarised ^{129}Xe ventilation MRI with standard lung physiological measurements in ILD patients in comparison to healthy volunteers (HV); secondly, to compare these MRI biomarkers between ILD subtypes; and thirdly, to assess longitudinal changes in these MRI biomarkers.

2. MATERIALS AND METHODS

2.1. Participants

The study was carried out as part of a programme to validate imaging biomarkers of drug safety [24]. It was conducted in accordance with the Declaration of Helsinki, and the

protocol was approved by the local research ethics committee (United Kingdom North West - Preston Research Ethics Committee, REC Ref 17/NW/0631, IRAS number: 232495). The study investigated several imaging biomarkers intended to probe lung morphology, perfusion, and ventilation. This report includes only the subgroup of patients in whom OE-MRI and ^{129}Xe ventilation MRI was performed.

Patients with a diagnosis of ILD were recruited and assigned to one of four ILD subtypes: suspected DI-ILD, connective tissue disease related-ILD (CTD-ILD), IPF or HP.

The diagnosis of the ILD subtype was established in ILD multidisciplinary team (MDT) meetings involving respiratory physicians, thoracic radiologists, and pathologists, the gold standard for the diagnosis of ILD since the publication of the ATS/ERS IIP classification in 2002 [25].

Potential subjects were identified by respiratory physicians during ILD MDT meetings where patients' cases were discussed as part of routine clinical care. Current diagnostic investigations in ILD mainly consist of HRCT and PFTs [25]. It should be noted that often a definitive diagnosis cannot be achieved by the MDT, but instead a "working diagnosis" of high probability can be reached by combining the key information available to increase or decrease the diagnostic probability of a specific ILD subtype [26]. As this was an observational trial, recruited patients followed the usual standard of care, but treatment regime was noted.

Exclusion criteria were: significant pre-existing cardio-pulmonary disease, radiotherapy to the lung fields within 6 months, any features of any malignancy involving the lungs, evidence of lower respiratory infection, estimated survival <6 months and any contraindication for MR imaging.

Patients were recruited, gave written informed consent, and underwent a clinical assessment, lung function testing and MRI at visit 1. Patients were recalled for a follow up visit after 6 weeks (if diagnosed with suspected DI-ILD or HP) or 6 months (if diagnosed with IPF or CTD-ILD). The follow up schedules were tailored to enable the capture of change at the most appropriate time points for each disease group, as IPF patients typically show a slower progressive decline while DI-ILD and HP often either rapidly declines or improves with treatment. Additionally, ten healthy volunteers (HV) were also recruited under ethical approval provided by the UK national research ethics committee (REC Ref 12/NE/0355),

with all volunteers giving written informed consent to undergo pulmonary function testing and MRI at baseline only.

2.2. Pulmonary function tests

Patients underwent pulmonary function testing prior to MRI scanning, performed to international standards [27] under the supervision of a trained respiratory physiologist. Spirometry was performed to assess the forced expiratory volume in 1 second (FEV_1) and forced vital capacity (FVC). Gas transfer testing assessed the transfer factor (TL_{CO}) and coefficient (K_{CO}) of the lungs for carbon monoxide [28,29]. All values are reported as % predicted using the Global Lung Function Initiative (GLI) 2012 reference equations [30].

2.3. Imaging

All imaging was carried out in the coronal plane on a 1.5 T whole body system (GE HDx, GE Healthcare, Milwaukee, WI): table 1 provides details of the sequences used.

2.3.1. Hyperpolarised ^{129}Xe imaging

Hyperpolarised ventilation ^{129}Xe imaging was performed using a flexible quadrature transmit/receive quadrature coil (Clinical MR Solutions, Brookfield, Wisconsin, USA). ^{129}Xe was polarised under regulatory licence to ~30% using an in-house spin exchange optical pumping polariser capable of generating 500 ml doses in less than 15 minutes [31]. ^{129}Xe images were acquired at a breath-hold of functional residual capacity plus 1 litre of gas mixture (FRC+1L, 500mL ^{129}Xe, 500mL N_2) with a 3D balanced steady-state free precession (bSSFP) sequence with a 10 mm slice thickness and pixel size of 4 mm x 4 mm. Prior to the acquisition of the ^{129}Xe images, a ^{1}H structural 3D spoiled gradient echo (SPGR) image was acquired at FRC+1L utilising a 1L bag of N_2. The ^{1}H structural image had the same in plane spatial resolution, but a slice thickness of 5 mm compared to 10 mm for the ^{129}Xe image to allow for an affine co-registration and the estimation of the percentage lung ventilated volume (Xe-VVF) [32]. To ensure all subjects were able to complete the breathing manoeuvre, appropriate training took place prior to imaging.

2.3.2. Inversion recovery T_1 measurement and dynamic Oxygen-enhanced imaging

Following completion of ^{129}Xe imaging, subjects were repositioned in an 8-element ^{1}H chest receiver coil and were fitted with a disposable non-rebreathing mask to allow for medical air and oxygen delivery. A free-breathing protocol based on an inversion-prepared centric

ordered single shot 3D-turbo field echo (IR-TFE) sequence was used [33] with 10 mm slice thickness and 4.2 mm x 4.2 mm spatial resolution. A baseline T_1 map was calculated from 6 acquisitions with variable inversion time (TI) (40, 100, 300, 1100, 2000 and 5000 ms). Five volumes were acquired for each TI, to capture different stages of the respiratory cycle. A dynamic OE acquisition followed, lasting 15 min (TI = 1100 ms) with a temporal resolution of 10 s, during which gas was delivered at 15 L/min and switched from medical air to 100% O_2 at minute 2, and back to air at minute 10 [34].

2.4. Image Analysis

2.4.1. ^{129}Xe image analysis

^{1}H structural images were co-registered to the same spatial domain as the ^{129}Xe ventilation image and segmented semi-automatically using spatial fuzzy c means thresholding and manual editing [31]. Xe-VVF was calculated by dividing the ventilated volume (from the ventilation image) by the thoracic cavity volume (from the ^{1}H structural image). Additionally, the median and interquartile range (IQR) of the coefficient of variation (CV) of ventilated signal intensity was calculated [35,36], with the IQR of the whole lung CV being referred to as the xenon ventilation heterogeneity index (Xe-VH_I). Briefly, for CV calculation the ^{129}Xe images were subsampled in-plane by 50% and a 3x3 sliding window used to calculate voxel-wise CV, incorporating only voxels identified as ventilated (from the ventilated volume mask).

2.4.2. Inversion recovery T_1 and dynamic Oxygen-enhanced imaging analysis

All OE-MRI images were co-registered using ANTS [37] to a reference image representing expiration. Baseline T_1 was calculated by fitting the inversion recovery data as previously described [34].

The lung cavity was semi-automatically segmented from the reference image using a region growing algorithm from manually defined points. Lung volume changes during the dynamic acquisition were estimated from the mask and the deformation field extracted from the registration. The registration was assessed by extracting the apparent diaphragm displacement from the dynamic images after motion-correction: any frame presenting an apparent post-correction displacement greater than 1 pixel was excluded from further analysis.

The dynamic signal at each pixel in the lung parenchyma was modelled by sum of two signals: (1) a component dependent on lung volume change, describing the local variation in local proton density during the respiratory cycle and (2) a piecewise mono-exponential

recovery function in the time domain, modelling the local increase in T_1-weighted MR signal due to an increase in concentration of dissolved molecular oxygen after gas switching.

To account for the first element, a first-degree polynomial fit between the log-transformed pixelwise MR signal and the log-transformed whole lung volume changes was calculated and subtracted from the original signal. The oxygen enhancement was then derived by the change in signal intensity between the median values on medical air and the median values of the last ten frames on 100% O_2. This signal change was then converted to the change in R_1 [38], and then into a change of partial pressure of oxygen (ΔpO_2), using the longitudinal relaxivity in water ($r_{1_{O_2}}$) of 2.49 × 10−4/s mmHg [39].

In line with the ^{129}Xe analysis, the median value of the coefficient of variation of the ΔpO_2 map (median CV ΔpO_2) was extracted by a 3 x 3 2D kernel. The interquartile range of this map was also calculated, as the oxygen enhanced ventilation heterogeneity index (OE-VH_I).

The oxygen wash in time (τ_{up}) was estimated by fitting the signal with a piecewise mono-exponential curve. When the Akaike information criterion (AIC) favoured the latter fitting over a constant function, the pixel was considered as ventilated, which allowed the calculation of the oxygen enhanced ventilated volume fraction (OE-VVF). The OE-VVF was applied to the τ_{up} map as a mask to exclude pixels with no detectable oxygen enhancement.

2.5. Statistics:

The five ^{1}H MRI biomarkers (T_1, ΔpO_2, τ_{up}, OE-VH_I and OE-VVF) and the two ^{129}Xe ventilation biomarkers (Xe-VVF and Xe-VH_I), were compared with the spirometry (FEV_1%, FVC%), and the gas transfer biomarker TL_{CO}%. To evaluate differences in biomarkers at visit 1 among the ILD subgroups and the healthy volunteers, ANOVA or Kruskal-Wallis rank tests followed by post hoc test with Bonferroni or Dunn correction for multiple comparisons were carried out (depending on the result of the Shapiro-Wilk normality test). The level of significance was set at p=0.05 for these tests after multiple correction.

Also, the considered population data at visit 1 was divided into three groups: healthy volunteers, ILD subject with TL_{CO}% > 75% (High TL_{CO}%) and ILD subject with TL_{CO}% <= 75% (LowTLCO%). A similar analysis to the one just described was carried out to determine if any imaging biomarker could separate HV from both High TL_{CO}% and LowTLCO% groups.

To assess the relationships between imaging biomarkers, Pearson correlations were carried out. Pearson correlations were also carried out between each of the imaging biomarkers and PFTs and age/gender, both at visit 1 and (separately) for the between visits change. The level of significance was set at p=0.01 for these tests. When at least one significant correlation was found, the best multilinear regression model was identified as having had the imaging biomarker as an independent parameter, the PFTs and age as a continuous covariate and sex and disease status (HV, IPF, DI-ILD, CTD-ILD, HP) as categorical variables, using a stepwise method guided by a decreasing Akaike Information Criterion. The results of the multivariate models are presented as the coefficient β and its 95% confidence interval and R^2, the percentage of variation in the response that is explained by the model.

To assess the change of PFT between visits in the whole population, and in each of the ILD subgroups, a one sample t-test or Wilcoxon signed rank test was carried out. The level of significance was set at p=0.01 for these tests. No correction for multiple comparisons was applied.

Moreover, subjects were divided in two groups depending on whether they received a pharmacological treatment for ILD during the study. The change in biomarker between visits was compared between the two groups with a two-tailed t-test or a Wilcoxon signed rank test depending on the result of the Shapiro normality test. The level of significance was set at p=0.01 for these tests. No correction for multiple comparisons was applied. All statistical analysis were run using Python libraries *SciPy* (version 1.6.0) and *statsmodels* (version 0.12.0).

3. Results:

Figure 1 shows one representative slice from all considered biomarker maps, ^{129}Xe biomarker, CT, and OE-MRI for an IPF subject. Figures 2 and 3 show a comparison of anterior-posterior slices from the ^{129}Xe volumetric acquisition and OE-MRI enhancement map and wash-in rate of a subject with HP and a patient with IPF. A clear gradient in ^{129}Xe spin density front-to-back is clearly visible in ^{129}Xe ventilation images. This gradient seems reversed in ΔpO_2 images, with posterior images enhancing less than anterior ones. In figure 2 ventilation is mostly uniform, but a ventilation defect visible on ^{129}Xe images is visible in the upper right lung and corresponds to normal ΔpO_2 enhancement but high τ_{up}. Apparent

artefacts are visible in the left lung, close to the heart, in OE-MRI images. In figure 3, significant differences in contrast in between modalities are clearly visible, but some commonality in ventilation defects are also evident (arrow, asterisk and plus signs).

3.1. **Population characteristics**

Figure 4 summarises in a flow chart the patient recruitment in the study. Forty-one ILD patients were recruited (14 IPF, 11 HP, 11 DI-ILD and 5 CTD-ILD) and successfully imaged at visit 1. Thirty-six complete datasets of ILD patients imaged at visit 1 were analysed (12 IPF, 10 HP, 11 DI-ILD and 3 CTD-ILD). Five subjects were not analysed; one subject due to the dynamic OE-MRI protocol not being fully performed and four subjects OE-MRI datasets were excluded due to absent or weak O_2 enhancement in the blood pool as measured in the aorta, which indicated issues with the gas delivery during scanning.

Thirty-four ILD patients attended and completed visit 2 (11 IPF, 8 HP, 10 DIILD, 5 CTD-ILD). Of the seven patients who failed to attend, three subjects died between visit 1 and visit 2, two withdrew from the study, one was lost at follow up and one could not be scanned in the appropriate time window due to MR hardware issues. One of the thirty-four acquisitions could not be analysed due to inconsistent field of view prescription among the OE acquisitions. No incidental findings were reported in the study population.

A total of twenty-nine ILD patients (nine IPF, ten HP, seven DILD, three CTD-ILD) completed both visits and had analysable OE-MRI datasets. One HV was excluded from the analysis due to due to a radiological incidental finding, and the remaining nine HV were analysed. Table 2 summarises biomarker results obtained at visit 1 and the change between visits (visit 2 – visit 1).

Regarding pharmacological treatment, in the IPF group, four subjects were treated with an antifibrotic (Nintedanib), while the remaining subjects were not under pharmacological treatment. Among the subjects diagnosed with HP, all were treated with a corticosteroid (prednisone); in addition to this, one HP patient also received Azathioprine (AZA) and four patients also received Mycophenolate Mofetil (MMF). In the CTD-ILD group, one subject received no pharmacological treatment during the study, two were on a corticosteroid plus AZA and two on a corticosteroid plus MMF. Among subjects diagnosed with DI-ILD, six received a corticosteroid, while five did not receive drugs for the condition as their

management plan involved withdrawal of the causative drug only. Starting, stopping and length of treatment also varied widely during the study.

3.2. PFTs and imaging biomarkers at visit 1

No difference was found in FEV_1% and FVC% between HV and any ILD subgroups. HV had higher TL_{CO}% ($p<0.001$) than all ILD groups, while HV had statistically higher K_{CO}% than IPF ($p<0.0001$), DI-ILD ($p=0.01$) and CTD-ILD ($p=0.01$), but not HP ($p=0.12$). There were no significant differences between ILD subgroups for these biomarkers (Figure 5). The subgroup considered differed in age: HV (HV: 49.4 ± 17.4 y) were significantly younger than the IPF (IPF: 71.9 ± 7.18 y, $p=0.004$). IPF patients were also older then CTD-ILD patients (58.5 ± 10.9 y, $p=0.04$) (Table 2).

Figure 6 presents the boxplot of the considered ^{129}Xe biomarkers and figure 7 presents the boxplot of the considered OE-MRI biomarkers, divided by ILD subgroups. Regarding ^{129}Xe biomarkers, the ventilation volume fraction was lower in all ILD groups than in HV (Xe-VVF: HV mean ± std 97.4 ± 2.6, CTD-ILD: 91.0 ± 4.8, p= 0.017, DI-ILD 90.1 ± 7.4 p=0.003, HP 92.6 ± 3.8 p= 0.013, IPF 88.1± 6.3 p<0.001), but this was not replicated with the OE ventilation volume fraction. As for PFTs, when averaged across the lung, the OE-MRI biomarkers generally failed to distinguish the ILD subgroups, with the exception that ΔpO_2 was higher in CTD-ILD than in IPF ($p=0.016$).

There were however significant differences in ventilation heterogeneity between ILD groups. Xe-VH_I was lower in HV than in IPF ($p<0.001$). Xe-VH_I was also lower in the CTD-ILD group than in IPF ($p<0.001$), and lower in HP than in IPF ($p=0.042$).

If visit 1 subjects are divided between HV, HighTLCO% and LowTLCO% groups, Xe-VVF was higher in HV than in both ILD groups (HV 97.38 ± 2.64, HighTLCO%: 94.11 ± 5.317, LowTLCO% 90.25 ± 6.38 %, HV vs High $p=0.002$, HV vs Low, $p<0.001$).
Xe-VH_I was significantly lower in HV (0.095 ± 0.013) than in LowTLCO% (0.123 ± 0.02, $p=0.006$), but not significantly different than in the HighTLCO% (0.105 ± 0.021).
Similarly, T_1 is higher in HV (1180.7 ± 95.5 ms) than in LowTLCO% (1103.4 ± 63.2 ms, $p=0.02$), but not than in HighTLCO% (1157.68 ± 83 ms). τ_{up} was lower in HV (38.77 ± 12.68 s) than in HighTLCO% (49.32 ± 20.18 s, $p=0.03$), but not significantly different than in LowTCLO% (48.8 ± 24.4 s).
Table 3 shows the Pearson correlation coefficients between imaging biomarkers at visit 1. No significant correlation was found between Xe-VVF and OE-VVF, nor between Xe-VH_I and

OE-VH_I. There was a weak but significant correlation between τ_{up} and VVF (R=-0.38, p=0.009).

Multilinear regression models applied to the whole considered population demonstrated that age (β=-0.2; 95%CI = -0.33, -0.11; p<0.001) and TL_{CO} (β=0.07; 95%CI = 0.005, 0.136; p=0.035) were significantly correlated with Xe-VVF (R^2=0.39).

Age (β=0.0007; 95%CI = 10^{-4}, 10^{-3}; p=0.001), TL_{CO} (β=-0.0003, 95%CI = 10^{-4}, 10^{-3}; p=0.013) and gender (β=0.019; 95%CI = 0.009, 0.031; p=0.001) were significantly correlated with Xe-VH_I (R^2 = 0.53).

Age (β=-2.32; 95%CI = -3.85, -0.79; p=0.004), FVC% (β=0.97, 95%CI = 0.13, 1.81; p=0.025), and IPF diagnosis (β=33.2; 95%CI = -14.53, 80.99; p=0.168) were correlated with T_1 (R^2 = 0.24). No other associations were observed. The full table of Pearson correlation coefficients is available in the Supplementary Materials (Table 1).

3.3. Changes between visits

Boxplots representing the longitudinal changes in the considered biomarkers are visualised in the Supplementary Materials figures 1, 2 and 3. Regarding longitudinal changes, no statistically significant changes were found in individual ILD subgroups or in the overall ILD population.

If the population is divided between subjects who received pharmacological treatment for ILD during the study, and subjects who did not, no significant difference in the biomarker changes were found between the two groups.

3.4. Multilinear models – imaging biomarkers (visit 2 – visit1)

Only age at visit 1 was a significant predictor of the change in VVF between visits (R^2=0.145; β= 0.2; 95%CI = 0.026, 0.44; p=0.029). Multilinear models indicated that change of FEV_1% was significantly correlated with the change in T_1 between visits (R^2=0.138, β = -0.47; 95%CI = -9.33, -0.157; p=0.043) but no further associations with MRI biomarkers were observed. The full table of Pearson correlation coefficients is available in the Supplementary Materials (Table 2).

4. Discussion

Despite the complexity of the imaging employed in the study, only 2 subjects withdrew, demonstrating the feasibility of multi-sequence MR acquisition in ILD, also in patients with severely deteriorated lung function. Issues with oxygen delivery during scanning were detected – methods to identify when gas delivery is failing during scanning may be helpful in the future to improve data quality.

In this study, none of the global measurements (PFT, average T_1, or any of the global OE-MRI or ^{129}Xe ventilation biomarkers) differentiated between ILD subtypes, although biomarkers of focal variation (OE-VH_I and Xe-VH_I) may show differences in ventilation heterogeneity between ILD subtypes. The importance of accurately and quickly classifying a subject's ILD subtype comes from the impact on the prognosis as well as the choice of the most effective treatment for the patient (e.g., immunosuppression versus antifibrotic therapy). The results from this study suggest that ventilation-only biomarkers are not suitable for this specific objective, nor to track the longitudinal changes. In fact, the longitudinal change in the imaging biomarkers did not correlate with PFT changes between the two timepoints. The significant correlation between τ_{up} and Xe-VVF suggests that areas of the lung not reached by ^{129}Xe during the breath-hold experiment may be reached by oxygen at a slower rate during the significantly longer free breathing OE-MRI experiment. This would also be consistent with the observation that, unlike Xe-VVF, the fraction of lung apparently ventilated by oxygen (OE-VVF) did not differentiate between groups.

The only imaging biomarker that could separate the healthy volunteers and both the high and low TLCO% groups was Xe-VVF, which indicates that a limited but progressive loss of ventilated volume may occur as disease progresses.

The ILD patients recruited at baseline had on average near normal FVC% and FEV_1%, but similar low TL_{CO}%; it is perhaps therefore unsurprising that functional imaging contrasts that are dominated by ventilation were unable to differentiate these groups [30]. Perhaps more surprisingly, as noted above, ventilated volume fractions did not correlate between OE-MRI and ^{129}Xe-MRI. In addition to the differences in the time scales over which the measurements are performed, this lack of correlation is possibly because OE-MRI measures signal enhancement in the parenchyma and blood in the lungs following oxygen ventilation, and is therefore best considered as creating contrast weighted by both ventilation and perfusion, while ventilation ^{129}Xe-MRI directly measures ventilation in the airways and the alveoli; alternatively, it may simply reflect the relative variability and small numbers in this work.

The OE-VVF obtained in this work is relatively low also in healthy volunteers (80.8 ± 9.8 %). Lack of enhancement is expected in bronchi and arteries in this imaging method, therefore reducing the achievable VVF to less than 100%. It is also possible that movement artefacts from breathing, the cardiac cycle and bulk movements may contribute to decreased OE-VVF.

Also, while both OE-MRI and ^{129}Xe-MRI suggested more heterogeneous ventilation in DI-ILD and IPF, ventilation heterogeneity index measurements failed to correlate between the two modalities, potentially for the same underlying reasons.

Correlation between Xe-VVF obtained with ^{3}He imaging and OE-VVF has been seen in a cystic fibrosis study [40] which did not investigate oxygen wash-in time. The lung pathology typical of CF is characterised by airway obstruction, leading to markedly decreased FEV_1 and FVC, markedly different from the fibrotic pathology present in ILD. Further studies are necessary to investigate the apparent distribution of different gases as visualised by MR imaging in an array of pulmonary diseases.

It is well known that ^{129}Xe ventilation biomarkers correlate strongly with age [41]. When age is considered in a multilinear model, Xe-VVF and VH_I are significantly correlated with TL_{CO} at visit 1. This result also indicates that reduction in ventilation volume and increase in ventilation heterogeneity in subjects with higher thickening of the alveolar-capillary membrane.

Sex is also independently correlated with VH_I, with female subjects presenting more uniformly ventilated lungs than male. Females are known to have a significant survival advantage in IPF [7], and this may be an additional indication of the mechanism behind this.

Lung T_1 correlated negatively with age, but sex was not found to predict T_1 in this population composed mostly of ILD patients. This can be compared with the findings of Kindval et al [42] who found a negative correlation between lung T_1 and age in female healthy volunteers. Lung T_1 also linearly correlated with FVC% when age is considered, and IPF patients present higher lung T_1 than the rest of the population. Stadler at al found that fibrotic patients in inspiration presented higher T_1 than emphysema patients [43], and this may explain the latter finding since the IPF population tends to present more as a fibrotic phenotype than other ILD types, and the acquisition was done in free breathing, so with inflated lungs.

The relationships found at visit 1 between imaging biomarkers and PFTs were mostly lost when considering short-term (6 weeks or 6 months) longitudinal changes. Among the ^{129}Xe ventilation biomarkers, the ventilated volume Xe-VVF change was significantly correlated only with age. Lung T_1 changes were negatively correlated with the change in FEV_1%. Since the change in PFTs between visits was small, this may explain the lack of correlation between imaging biomarkers and PFTs.

A limitation of this work is that, as a sub study, it was not adequately powered to address every question discussed here. Furthermore, the subjects were not uniformly distributed across the disease groups, reflecting challenges with the recruitment of rarer ILD variants. It is therefore possible that a larger study would uncover additional relationships. Subacute hypersensitivity pneumonitis is characterised by air trapping [41], so this subgroup may have been expected to have lower ventilated volume fractions than other ILD subtypes, but this was not found in this population. Also, the age differences between healthy volunteers and the IPF group is a potential issue. Potential further development within the field may also lead to a growing understanding of the imaging techniques and further insights into disease pathology, physiology and progression may develop over time with increasing experience and patient numbers.

Another limitation regards the observational nature of the study. Subjects received varied treatment regimens before and after recruitment, due to the different origin of ILD and a wide range of disease severity. Also, the timing of the baseline study visits in relation to the management of non-IPF subjects varied between the two centres. It is possible that the variation in the patient management in the study could have influenced the longitudinal changes in the biomarkers and a more standardised approach may have resulted in different outcomes. Therefore, the failures of the imaging biomarkers in distinguishing longitudinal changes between the group receiving or not pharmacological treatment must be interpreted cautiously.

Another limitation of our work is its focus on imaging techniques that are centred around ventilation imaging. There exist alternative techniques, such as spectroscopy and diffusion-weighted ^{129}Xe MRI [9,14,45] or ^{1}H perfusion MRI [46], which are capable of probing other lung properties such as gas exchange, lung microstructure and blood perfusion. Such measurements provide a promising alternative class of imaging biomarkers for ILD.

5. Conclusions

In conclusion, none of the global measurements investigated in this study were able to differentiate between ILD subtypes, suggesting that ventilation-only biomarkers are not indicated for this task. Limited but progressive loss of ventilated volume as measured by ^{129}Xe-MRI may be present as disease progresses, but no ventilation biomarker investigated in this study is a good candidate for monitoring longitudinal changes in ILD. ^{129}Xe ventilation biomarkers correlated strongly with age and TL_{CO} at visit 1, but the correlations were mostly lost when considering short-term (6 weeks or 6 months) longitudinal changes.

Both OE-MRI and ^{129}Xe MRI revealed more spatially heterogeneous ventilation in DI-ILD and IPF.

ACKNOWLEDGEMENTS

The research leading to these results received funding from the Innovative Medicines Initiatives 2 Joint Undertaking under grant agreement No 116106. This Joint Undertaking receives support from the European Union's Horizon 2020 research and innovation programme and EFPIA. This work was also supported by the National Institute of Health Research (RP-R3-12-027), Medical Research Council (MR/M008894/1) and GlaxoSmithKline (PJCH:BIDS3000032592). The views expressed are those of the authors and not necessarily those of the NHS, NIHR, the Department of Health, GlaxoSmithKline nor the TRISTAN consortium.

REFERENCES

1. Skeoch, S.; Weatherley, N.; Swift, A.J.; Oldroyd, A.; Johns, C.; Hayton, C.; Giollo, A.; Wild, J.M.; Waterton, J.C.; Buch, M. Drug-Induced Interstitial Lung Disease: A Systematic Review. *J Clin Med* **2018**, *7*, 356.
2. Vasakova, M.; Morell, F.; Walsh, S.; Leslie, K.; Raghu, G. Hypersensitivity Pneumonitis: Perspectives in Diagnosis and Management. *American Journal of Respiratory and Critical Care Medicine* **2017**, *196*, doi:10.1164/rccm.201611-2201PP.
3. Travis, W.D.; Costabel, U.; Hansell, D.M.; King, T.E.; Lynch, D.A.; Nicholson, A.G.; Ryerson, C.J.; Ryu, J.H.; Selman, M.; Wells, A.U.; et al. An Official American Thoracic Society/European Respiratory Society Statement: Update of the International Multidisciplinary Classification of the Idiopathic Interstitial Pneumonias. *American Journal of Respiratory and Critical Care Medicine* **2013**, *188*, doi:10.1164/rccm.201308-1483ST.

4. Ley, B.; Swigris, J.; Day, B.; Stauffer, J.L.; Raimundo, K.; Chou, W.; Collard, H.R. Pirfenidone Reduces Respiratory-Related Hospitalizations in Idiopathic Pulmonary Fibrosis. *American Journal of Respiratory and Critical Care Medicine* **2017**, *196*, doi:10.1164/rccm.201701-0091OC.
5. Bernstein, E.J.; Jaafar, S.; Assassi, S.; Domsic, R.T.; Frech, T.M.; Gordon, J.K.; Broderick, R.J.; Hant, F.N.; Hinchcliff, M.E.; Shah, A.A.; et al. Performance Characteristics of Pulmonary Function Tests for the Detection of Interstitial Lung Disease in Adults With Early Diffuse Cutaneous Systemic Sclerosis. *Arthritis & Rheumatology* **2020**, *72*, doi:10.1002/art.41415.
6. Weatherley, N.D.; Eaden, J.A.; Stewart, N.J.; Bartholmai, B.J.; Swift, A.J.; Bianchi, S.M.; Wild, J.M. Experimental and Quantitative Imaging Techniques in Interstitial Lung Disease. *Thorax* **2019**, *74*, doi:10.1136/thoraxjnl-2018-211779.
7. Ley, B.; Collard, H.R.; King Jr, T.E. Clinical Course and Prediction of Survival in Idiopathic Pulmonary Fibrosis. *Am J Respir Crit Care Med* **2011**, *183*, 431–440.
8. Daccord, C.; Maher, T.M. Recent Advances in Understanding Idiopathic Pulmonary Fibrosis. *F1000Res* **2016**, *5*, doi:10.12688/f1000research.8209.1.
9. Weatherley, N.D.; Stewart, N.J.; Chan, H.-F.; Austin, M.; Smith, L.J.; Collier, G.; Rao, M.; Marshall, H.; Norquay, G.; Renshaw, S.A.; et al. Hyperpolarised Xenon Magnetic Resonance Spectroscopy for the Longitudinal Assessment of Changes in Gas Diffusion in IPF. *Thorax* **2019**, *74*, doi:10.1136/thoraxjnl-2018-211851.
10. He, M.; Zha, W.; Tan, F.; Rankine, L.; Fain, S.; Driehuys, B. A Comparison of Two Hyperpolarized 129Xe MRI Ventilation Quantification Pipelines: The Effect of Signal to Noise Ratio. *Academic Radiology* **2019**, *26*, doi:10.1016/j.acra.2018.08.015.
11. He, M.; Driehuys, B.; Que, L.G.; Huang, Y.-C.T. Using Hyperpolarized 129Xe MRI to Quantify the Pulmonary Ventilation Distribution. *Academic Radiology* **2016**, *23*, doi:10.1016/j.acra.2016.07.014.
12. Stewart, N.J.; Norquay, G.; Griffiths, P.D.; Wild, J.M. Feasibility of Human Lung Ventilation Imaging Using Highly Polarized Naturally Abundant Xenon and Optimized Three-Dimensional Steady-State Free Precession. *Magnetic Resonance in Medicine* **2015**, *74*, doi:10.1002/mrm.25732.
13. Stewart, N.J.; Chan, H.; Hughes, P.J.C.; Horn, F.C.; Norquay, G.; Rao, M.; Yates, D.P.; Ireland, R.H.; Hatton, M.Q.; Tahir, B.A. Comparison of 3He and 129Xe MRI for Evaluation of Lung Microstructure and Ventilation at 1.5 T. *Journal of magnetic resonance imaging* **2018**, *48*, 632–642.
14. Kern, A.L.; Gutberlet, M.; Qing, K.; Voskrebenzev, A.; Klimeš, F.; Kaireit, T.F.; Czerner, C.; Biller, H.; Wacker, F.; Ruppert, K.; et al. Regional Investigation of Lung Function and Microstructure Parameters by Localized ^{129} Xe Chemical Shift Saturation Recovery and Dissolved-Phase Imaging: A Reproducibility Study. *Magnetic Resonance in Medicine* **2019**, *81*, doi:10.1002/mrm.27407.
15. Kaushik, S.S.; Robertson, S.H.; Freeman, M.S.; He, M.; Kelly, K.T.; Roos, J.E.; Rackley, C.R.; Foster, W.M.; McAdams, H.P.; Driehuys, B. Single-Breath Clinical Imaging of Hyperpolarized ^{129} Xe in the Airspaces, Barrier, and Red Blood Cells Using an Interleaved 3D Radial 1-Point Dixon Acquisition. *Magnetic Resonance in Medicine* **2016**, *75*, doi:10.1002/mrm.25675.
16. Collier, G.J.; Eaden, J.A.; Hughes, P.J.C.; Bianchi, S.M.; Stewart, N.J.; Weatherley, N.D.; Norquay, G.; Schulte, R.F.; Wild, J.M. Dissolved ^{129} Xe Lung MRI with Four-echo 3D Radial Spectroscopic Imaging: Quantification of Regional Gas Transfer in Idiopathic Pulmonary Fibrosis. *Magnetic Resonance in Medicine* **2021**, *85*, doi:10.1002/mrm.28609.

17. Kern, A.L.; Vogel-Claussen, J. Hyperpolarized Gas MRI in Pulmonology. *The British Journal of Radiology* **2018**, doi:10.1259/bjr.20170647.
18. Renne, J.; Lauermann, P.; Hinrichs, J.; Schönfeld, C.; Sorrentino, S.; Gutberlet, M.; Jakob, P.; Wacker, F.; Vogel-Claussen, J. Clinical Use of Oxygen-Enhanced T_1 Mapping MRI of the Lung: Reproducibility and Impact of Closed versus Loose Fit Oxygen Delivery System. *Journal of Magnetic Resonance Imaging* **2015**, *41*, doi:10.1002/jmri.24535.
19. Edelman, R.R.; Hatabu, H.; Tadamura, E.; Li, W.; Prasad, P. v Noninvasive Assessment of Regional Ventilation in the Human Lung Using Oxygen-Enhanced Magnetic Resonance Imaging. *Nat Med* **1996**, *2*, 1236–1239, doi:10.1038/nm1196-1236.
20. Martini, K.; Gygax, C.M.; Benden, C.; Morgan, A.R.; Parker, G.J.M.; Frauenfelder, T. Volumetric Dynamic Oxygen-Enhanced MRI (OE-MRI): Comparison with CT Brody Score and Lung Function in Cystic Fibrosis Patients. *Eur Radiol* **2018**, *28*, 4037–4047, doi:10.1007/s00330-018-5383-5.
21. Ohno, Y.; Yui, M.; Yoshikawa, T.; Seki, S.; Takenaka, D.; Kassai, Y.; Hattori, H.; Murayama, K.; Toyama, H. 3D Oxygen-Enhanced MRI at 3T MR System: Comparison With Thin-Section CT of Quantitative Capability for Pulmonary Functional Loss Assessment and Clinical Stage Classification of COPD in Smokers. *J Magn Reson Imaging* **2021**, *53*, 1042–1051, doi:10.1002/jmri.27441.
22. Triphan, S.M.F.; Stahl, M.; Jobst, B.J.; Sommerburg, O.; Kauczor, H.; Schenk, J.; Alrajab, A.; Eichinger, M.; Mall, M.A.; Wielpütz, M.O. Echo Time-Dependence of Observed Lung <scp> T_1 </Scp> in Patients With Cystic Fibrosis and Correlation With Clinical Metrics. *Journal of Magnetic Resonance Imaging* **2020**, *52*, doi:10.1002/jmri.27271.
23. Triphan, S.M.F.; Jobst, B.J.; Anjorin, A.; Sedlaczek, O.; Wolf, U.; Terekhov, M.; Hoffmann, C.; Ley, S.; Düber, C.; Biederer, J.; et al. Reproducibility and Comparison of Oxygen-Enhanced T1 Quantification in COPD and Asthma Patients. *PLOS ONE* **2017**, *12*, doi:10.1371/journal.pone.0172479.
24. https://www.imi-tristan.eu/ TRISTAN .
25. American Thoracic Society; European Respiratory Society American Thoracic Society/European Respiratory Society International Multidisciplinary Consensus Classification of the Idiopathic Interstitial Pneumonias. This Joint Statement of the American Thoracic Society (ATS), and the European Respiratory Society (ERS) Was Adopted by the ATS Board of Directors, June 2001 and by the ERS Executive Committee, June 2001. *Am J Respir Crit Care Med* **2002**, *165*, 277–304, doi:10.1164/ajrccm.165.2.ats01.
26. Lynch, D.A.; Sverzellati, N.; Travis, W.D.; Brown, K.K.; Colby, T. v; Galvin, J.R.; Goldin, J.G.; Hansell, D.M.; Inoue, Y.; Johkoh, T.; et al. Diagnostic Criteria for Idiopathic Pulmonary Fibrosis: A Fleischner Society White Paper. *Lancet Respir Med* **2018**, *6*, 138–153, doi:10.1016/S2213-2600(17)30433-2.
27. Miller, M.R.; Hankinson, J.; Brusasco, V.; Burgos, F.; Casaburi, R.; Coates, A.; Crapo, R.; Enright, P. vd; van der Grinten, C.P.M.; Gustafsson, P. Standardisation of Spirometry. *European respiratory journal* **2005**, *26*, 319–338.
28. Norquay, G.; Collier, G.J.; Rao, M.; Stewart, N.J.; Wild, J.M. Xe 129-Rb Spin-Exchange Optical Pumping with High Photon Efficiency. *Phys Rev Lett* **2018**, *121*, 153201.
29. Graham, B.L.; Brusasco, V.; Burgos, F.; Cooper, B.G.; Jensen, R.; Kendrick, A.; MacIntyre, N.R.; Thompson, B.R.; Wanger, J. 2017 ERS/ATS Standards for Single-

Breath Carbon Monoxide Uptake in the Lung. *European Respiratory Journal* **2017**, *49*, 1600016.

30. Quanjer, P.H.; Stanojevic, S.; Cole, T.J.; Baur, X.; Hall, G.L.; Culver, B.H.; Enright, P.L.; Hankinson, J.L.; Ip, M.S.M.; Zheng, J.; et al. Multi-Ethnic Reference Values for Spirometry for the 3–95-Yr Age Range: The Global Lung Function 2012 Equations. *European Respiratory Journal* **2012**, *40*, doi:10.1183/09031936.00080312.
31. Hughes, P.J.C.; Horn, F.C.; Collier, G.J.; Biancardi, A.; Marshall, H.; Wild, J.M. Spatial Fuzzy C-means Thresholding for Semiautomated Calculation of Percentage Lung Ventilated Volume from Hyperpolarized Gas and 1H MRI. *Journal of Magnetic Resonance Imaging* **2018**, *47*, 640–646.
32. Smith, L.J.; Horsley, A.; Bray, J.; Hughes, P.J.C.; Biancardi, A.; Norquay, G.; Wildman, M.; West, N.; Marshall, H.; Wild, J.M. The Assessment of Short- and Long-Term Changes in Lung Function in Cystic Fibrosis Using ^{129} Xe MRI. *European Respiratory Journal* **2020**, *56*, 2000441, doi:10.1183/13993003.00441-2020.
33. Ulloa, J.; Morgan, A.; Parker, G. Evaluation of Whole Lung 3D Dynamic Oxygen-Enhanced MRI. *European Respiratory Journal* **2014**, *44*, 1724.
34. Zhang, W.-J.; Niven, R.M.; Young, S.S.; Liu, Y.-Z.; Parker, G.J.M.; Naish, J.H. Dynamic Oxygen-Enhanced Magnetic Resonance Imaging of the Lung in Asthma—Initial Experience. *Eur J Radiol* **2015**, *84*, 318–326.
35. Woodhouse, N.; Wild, J.M.; Paley, M.N.J.; Fichele, S.; Said, Z.; Swift, A.J.; van Beek, E.J.R. Combined Helium-3/Proton Magnetic Resonance Imaging Measurement of Ventilated Lung Volumes in Smokers Compared to Never-smokers. *Journal of Magnetic Resonance Imaging: An Official Journal of the International Society for Magnetic Resonance in Medicine* **2005**, *21*, 365–369.
36. Maunder, A.; Rao, M.; Robb, F.; Wild, J.M. Optimization of Steady-state Free Precession MRI for Lung Ventilation Imaging with 19F C3F8 at 1.5 T and 3T. *Magn Reson Med* **2019**, *81*, 1130–1142.
37. Avants, B.B.; Tustison, N.J.; Stauffer, M.; Song, G.; Wu, B.; Gee, J.C. The Insight ToolKit Image Registration Framework. *Frontiers in Neuroinformatics* **2014**, *8*, doi:10.3389/fninf.2014.00044.
38. Morgan, A.R.; Parker, G.J.M.; Roberts, C.; Buonaccorsi, G.A.; Maguire, N.C.; Hubbard Cristinacce, P.L.; Singh, D.; Vestbo, J.; Bjermer, L.; Jögi, J.; et al. Feasibility Assessment of Using Oxygen-Enhanced Magnetic Resonance Imaging for Evaluating the Effect of Pharmacological Treatment in COPD. *European Journal of Radiology* **2014**, *83*, doi:10.1016/j.ejrad.2014.08.004.
39. Dietrich, O.; Gaass, T.; Reiser, M.F. T1 Relaxation Time Constants, Influence of Oxygen, and the Oxygen Transfer Function of the Human Lung at 1.5 T—A Meta-Analysis. *European Journal of Radiology* **2017**, *86*, doi:10.1016/j.ejrad.2016.11.027.
40. Zha, W.; Kruger, S.J.; Johnson, K.M.; Cadman, R. v.; Bell, L.C.; Liu, F.; Hahn, A.D.; Evans, M.D.; Nagle, S.K.; Fain, S.B. Pulmonary Ventilation Imaging in Asthma and Cystic Fibrosis Using Oxygen-Enhanced 3D Radial Ultrashort Echo Time MRI. *Journal of Magnetic Resonance Imaging* **2018**, *47*, doi:10.1002/jmri.25877.
41. Virgincar, R.S.; Cleveland, Z.I.; Sivaram Kaushik, S.; Freeman, M.S.; Nouls, J.; Cofer, G.P.; Martinez-Jimenez, S.; He, M.; Kraft, M.; Wolber, J. Quantitative Analysis of Hyperpolarized 129Xe Ventilation Imaging in Healthy Volunteers and Subjects with Chronic Obstructive Pulmonary Disease. *NMR in Biomedicine* **2013**, *26*, 424–435.
42. Kindvall, S.S.I.; Diaz, S.; Svensson, J.; Wollmer, P.; Slusarczyk, D.; Olsson, L.E. Influence of Age and Sex on the Longitudinal Relaxation Time, T1, of the Lung in Healthy Never-smokers. *Journal of Magnetic Resonance Imaging* **2016**, *43*, 1250–1257.

43. Stadler, A.; Jakob, P.M.; Griswold, M.; Stiebellehner, L.; Barth, M.; Bankier, A.A. T1 Mapping of the Entire Lung Parenchyma: Influence of Respiratory Phase and Correlation to Lung Function Test Results in Patients with Diffuse Lung Disease. *Magn Reson Med* **2008**, *59*, 96–101, doi:10.1002/mrm.21446.
44. Magee, A.L.; Montner, S.M.; Husain, A.; Adegunsoye, A.; Vij, R.; Chung, J.H. Imaging of Hypersensitivity Pneumonitis. *Radiol Clin North Am* **2016**, *54*, 1033–1046, doi:10.1016/j.rcl.2016.05.013.
45. Kaushik, S.S.; Freeman, M.S.; Yoon, S.W.; Liljeroth, M.G.; Stiles, J. v.; Roos, J.E.; Michael Foster, W.S.; Rackley, C.R.; McAdams, H.P.; Driehuys, B. Measuring Diffusion Limitation with a Perfusion-Limited Gas—Hyperpolarized ^{129} Xe Gas-Transfer Spectroscopy in Patients with Idiopathic Pulmonary Fibrosis. *Journal of Applied Physiology* **2014**, *117*, doi:10.1152/japplphysiol.00326.2014.
46. Weatherley, N.D.; Eaden, J.A.; Hughes, P.J.C.; Austin, M.; Smith, L.; Bray, J.; Marshall, H.; Renshaw, S.; Bianchi, S.M.; Wild, J.M. Quantification of Pulmonary Perfusion in Idiopathic Pulmonary Fibrosis with First Pass Dynamic Contrast-Enhanced Perfusion MRI. *Thorax* **2021**, *76*, doi:10.1136/thoraxjnl-2019-214375.

Table 1. Imaging parameters for ^{129}Xe and OE acquisitions. SPGR: spoiled gradient echo, SSFP: steady state free precession, IR-TFE inversion recovery turbo spin echo, TE: echo time, TR: repetition time

Metric	^{1}H (SPGR)	^{129}Xe ventilation (SSFP)	T_1 Mapping (IR-TFE)	Dynamic OE (IR-TFE)
Acquisition matrix	100x100	100x80	96x96	96x96
Pixel size (mm^2)	4x4	4x4	4.2x4.2	4.2x4.2
Slice thickness (mm)	5	10	10	10
Flip angle (degrees)	5	10	5	5
TE/TR (ms)	0.6/1.9	2.2/6.7	0.4/1.5	0.4/1.5
BW (kHz)	±83.3	±8.0	±31.25	±31.25

Table 2. Summary statistics of age, lung test and image biomarkers at visit 1 (v1) and their change between visit 1 and visit 2 for all subjects involved in the study (v2-v1). IPF: idiopathic pulmonary fibrosis, DIILD: drug induced interstitial lung disease, CTD-ILD: connective tissue

disease-associated interstitial lung disease, HP: hypersensitivity pneumonitis, HV: healthy volunteers, FEV_1: forced expiratory volume in one second, FVC: forced vital capacity, TL_{CO}: transfer capacity of the lung for the uptake of carbon monoxide, K_{CO}: carbon monoxide transfer coefficient, Xe-VVF: percentage of ventilated volume as calculated by ^{129}Xe MRI, Xe-VH_I: ventilation heterogeneity index, ΔpO_2: change in oxygen partial pressure, $\tau_{up:}$ wash-in rate of oxygen, OE-VVF: ventilated volume as calculated by oxygen-enhanced MRI, OE-VH_I: ventilation heterogeneity index as calculated by oxygen-enhanced MRI, T_1: inversion recovery T_1, v1: visit 1, (v2-v1) difference between visit 2 and visit 1

	DIILD Visit 1 n=11 Visit 2 n=9	IPF Visit 1 n=14 Visit 2 n=9	HP Visit 1 n=11 Visit 2 n=7	CTD-ILD Visit 1 n=5 Visit 2 n=5	HV Visit 1 n=9
Male/female v1	8/3	13/1	3/8	3/2	6/3
Age [y]	66.4 ± 9.6	71.9 ± 7.18	61.5 ± 12.5	58.5 ± 10.9	49.4 ± 17.4
FEV1% *v1*	84.2 ± 24.0	93.5 ± 23.5	74.4 ± 24.4	89.[illegible] ± 11.0	95.2 ± 10.7
FEV1% (*v2- v1)*	-2.4 ± 9.3	-2.2 ± 7.3	2.6 ± 4.2	-0.[illegible] ± 5.5	
FVC% *v1*	82.9 ± 24.4	92.8 ± 26.4	74.1 ± 25.[illegible]	88.1 ± 12.7	101.4 ± 9.6
FVC% (*v2- v1)*	-2.2 ± 8.4	-3.8 ± 8.3	3.2 ± 4.[illegible]	-0.6 ± 5.4	
TL_{CO}% *v1*	56.0 ± 21.6	55.3 ± 18.6	56.4 ± 18.[illegible]	57.4 ± 19.6	97.6 ± 8.6
TL_{CO}% (*v2- v1)*	-1.1 ± 9.5	-5.4 ± 0.0	-3.6 ± [illegible].7	4.2 ± 4.6	
K_{CO}% *v1*	72.0 ± 21.8	69.8 ± 19.1	8[illegible].9 ± 22.1	72.0 ± 12.7	105.7 ± 13.5
K_{CO}% (*v2- v1)*	-2.21 ± 8.0	-5.2 ± 8.3	-[illegible]2.3 ± 20.6	1.5 ± 5.7	
Xe-VVF *v1*	90.1 ± 7.4	88.1 ± 6.5	92.6 ± 4.0	91.0 ± 4.8	97.4 ± 2.6
Xe-VVF (*v2- v1)*	1.2 ± 5.3	-0.22 ± [illegible]	-1.2 ± 5.1	0.58 ± 8.3	
Xe-VH_I *v1*	0.12 ± 0.03	0.1[illegible] ± 0.01	0.11 ± 0.03	0.11 ± 0.01	0.09 ± 0.01
Xe-VH_I (*v2- v1)*	0.00 ± 0.02	-0.0[illegible] ± 0.01	0.00 ± 0.1	0.00 ± 0.02	
Δ pO_2 [mmHg] *v1*	172.3 ± 48.2	141.6 ± 43.9	187.1 ± 41.9	244.6 ± 18.6	186.8 ± 48.4
Δ pO_2 [mmHg] (*v2- v1)*	-20.8 ± 56.4	33.5 ± 69.9	-0.6 ± 56.9	-64.4 7± 7.9	
τ_{up}[s] v1	60.2 ± 26.6	47.4 ± 19.1	44.9 ± 24.1	58.5 ± 41.6	38.8 ± 13.4
τ_{up}[s] (*v2- v1)*	-2.5 ± [illegible]	4.5 ± 35.0	-22.9 ± 18.1	-19.7 ± 33.3	
OE-VVF *v1*	[illegible]	69.2 ± 13.6	82.4 ± 9.9	88.6 ± 3.6	80.8 ± 9.8
OE-VVF (*v2- v1)*	-6.5 ± 10.4	7.5 ± 8.5	-0.0 ± 0.1	-10.9 ±7.6	
OE-VH_I *v1*	0.35 ± 0.10	0.40 ± 0.01	0.26 ± 0.12	0.22 ± 0.03	0.27 ± 0.13
OE-VH_I (*v2- v1)*	0.06. ± 1.0	-0.07 ± 0.06	3.7 ± 6.5	0.13 ± 0.1	
T_1 [ms] *v1*	1095.8 ± 55.9	1135.4 ± 47.4	1097.4 ± 78.3	1072.6 ± 41.8	1180.8 ± 95.5
T_1 [ms] (*v2- v1)*	40.3 ± 104.5	15.7 ± 89.3	38.9 ± 63.7	75.4 ± 110.7	

Table 3. Pearson correlation R between ventilation ^{129}Xe and OE-MRI biomarkers at visit 1. P values are indicated when p<0.05. Xe-VVF: percentage of ventilated volume as calculated by ^{129}Xe MRI; Xe-VH_I: ventilation heterogeneity index as calculated by ^{129}Xe MRI; Xe-VH_I: ventilation heterogeneity index as calculated by ^{129}Xe MRI; ΔpO_2: change in oxygen partial pressure; $\tau_{up:}$ wash-in rate of oxygen, OE-VVF: ventilated volume as calculated by oxygen-enhanced MRI, OE-VH_I: ventilation heterogeneity index as calculated by oxygen-enhanced MRI, T_1: proton longitudinal relaxation time.

	Xe-VVF	**Xe-VH_I**
T_1 [ms]	0.15	-0.34 (p=0.044)
ΔpO_2 [mmHg]	0.02	-0.05
OE-VH_I	-0.02	0.22
τ_{up}[s]	-0.38 (p=0.009)	0.34 (p=0.021)
OE-VVF	0.07	-0.23

Figures

Figure 1: Comparison of obtained images from ^{129}Xe ventilation (first row, with CT) and T1 and OE-MRI (second row) in a single slice for a subject diagnosed with IPF (FEV1% 85.8, FVC% 66.3, T_{LCO}% 26.6, K_{CO}% 44).

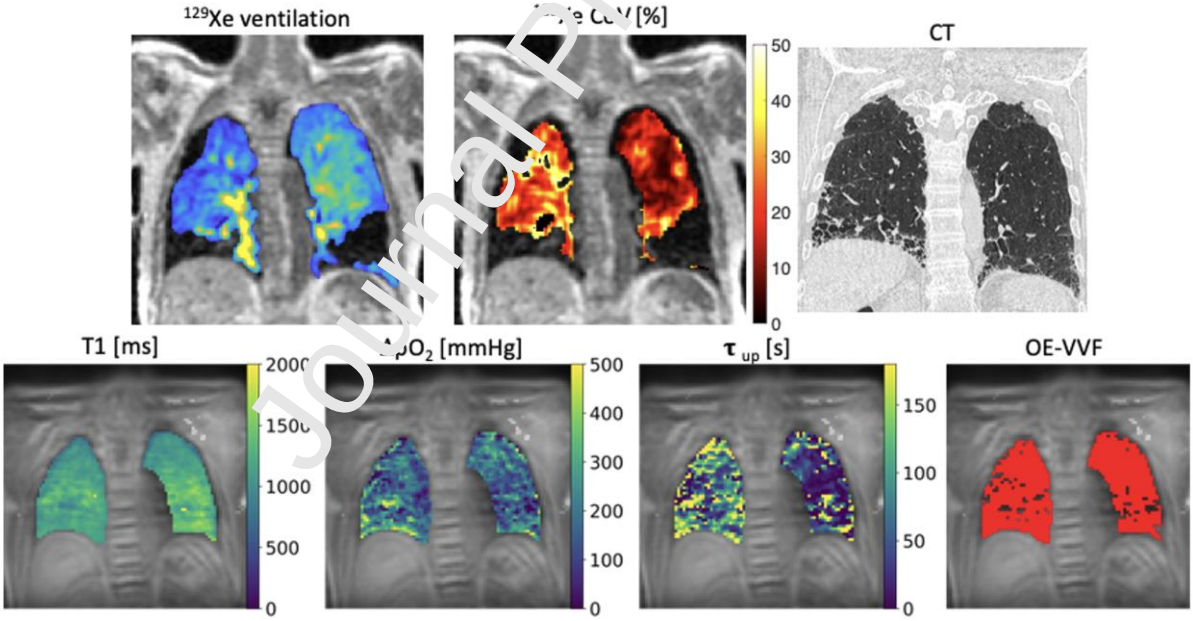

Figure 2: Front to back slice by slice comparison of ^{129}Xe images (first row) and OE-MRI delta pO_2 enhancement (second row) and oxygen wash in rate (third row) a subject affected by Hypersensitive Pneumonitis. Ventilation appears to be fairly homogeneous with both modalities. The main ventilation defect visible on the ^{129}Xe images is located in the upper right lobe and indicated by an asterisk. The same area presents normal oxygen enhancement levels but high oxygen wash-in rate. Apparent artefacts are visible close to the hearth in the left lung in OE-MRI images. [19]

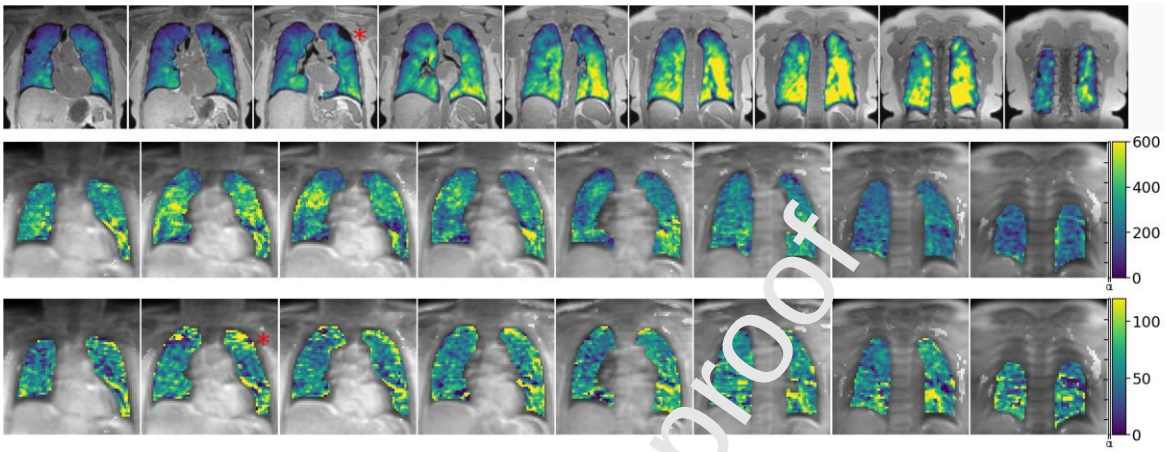

Figure 3: Front to back slice by slice comparison of ^{129}Xe images (first row) and OE-MRI delta pO_2 enhancement (second row) and oxygen wash in rate (third row) a subject affected by idiopathic pulmonary fibrosis. Significant differences in contrast between modalities are clearly visible, but some commonality in ventilation defects are also evident (arrow, asterisk and plus signs).

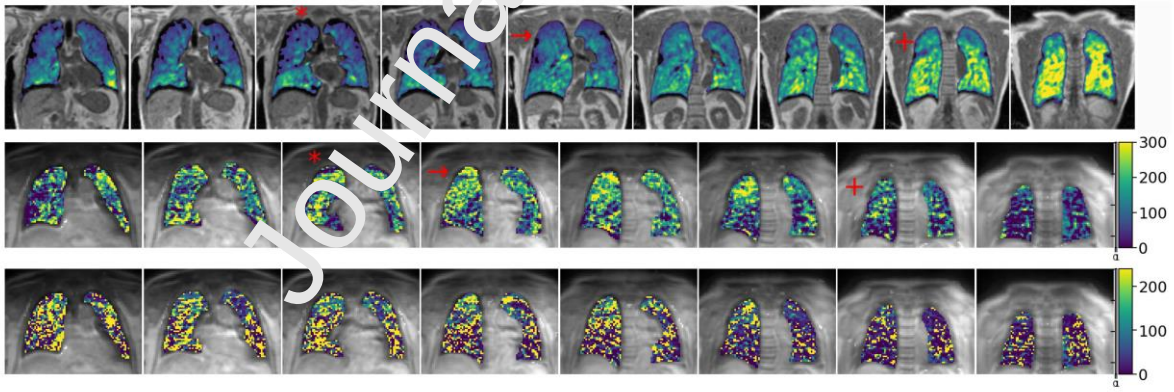

Figure 4: Flow chart representing patient recruitment during the study.

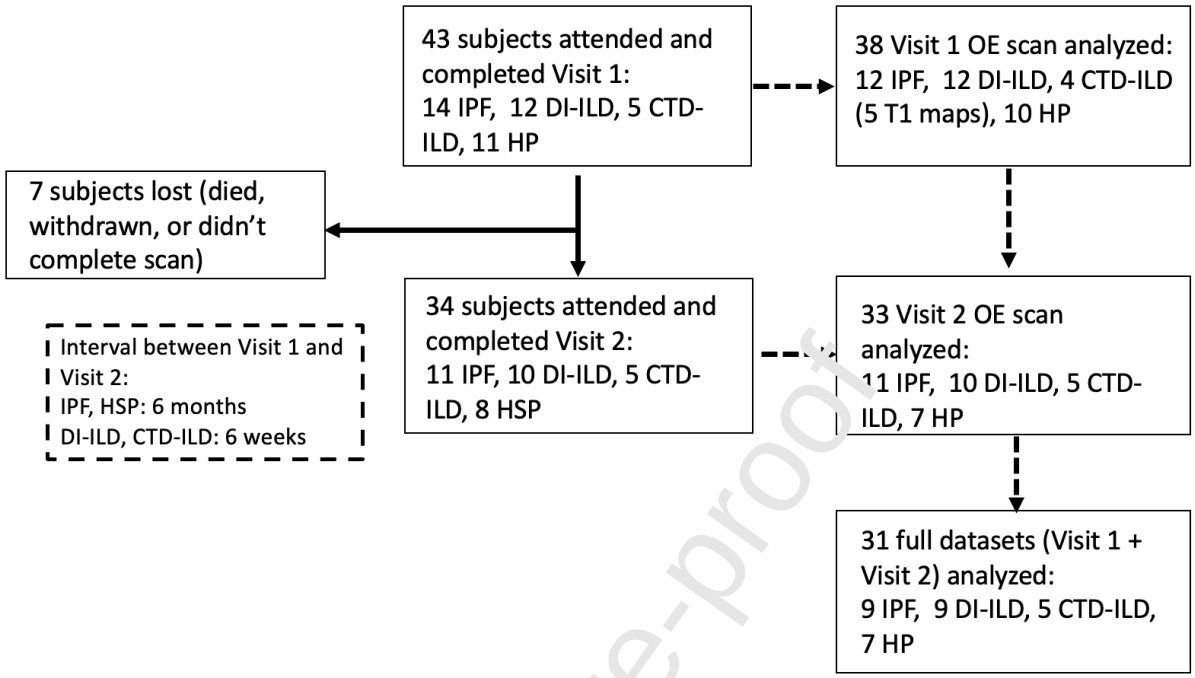

Figure 5: boxplot of pulmonary function tests results at visit 1 in the studied population, split in ILD subgroups. Data are reported as % predicted. (*) p<0.05, (***) p<0.001

FEV_1: forced expiratory volume in one second, FVC: forced vital capacity, TL_{CO}: transfer capacity of the lung for the uptake of carbon monoxide, K_{CO}: carbon monoxide transfer coefficient,

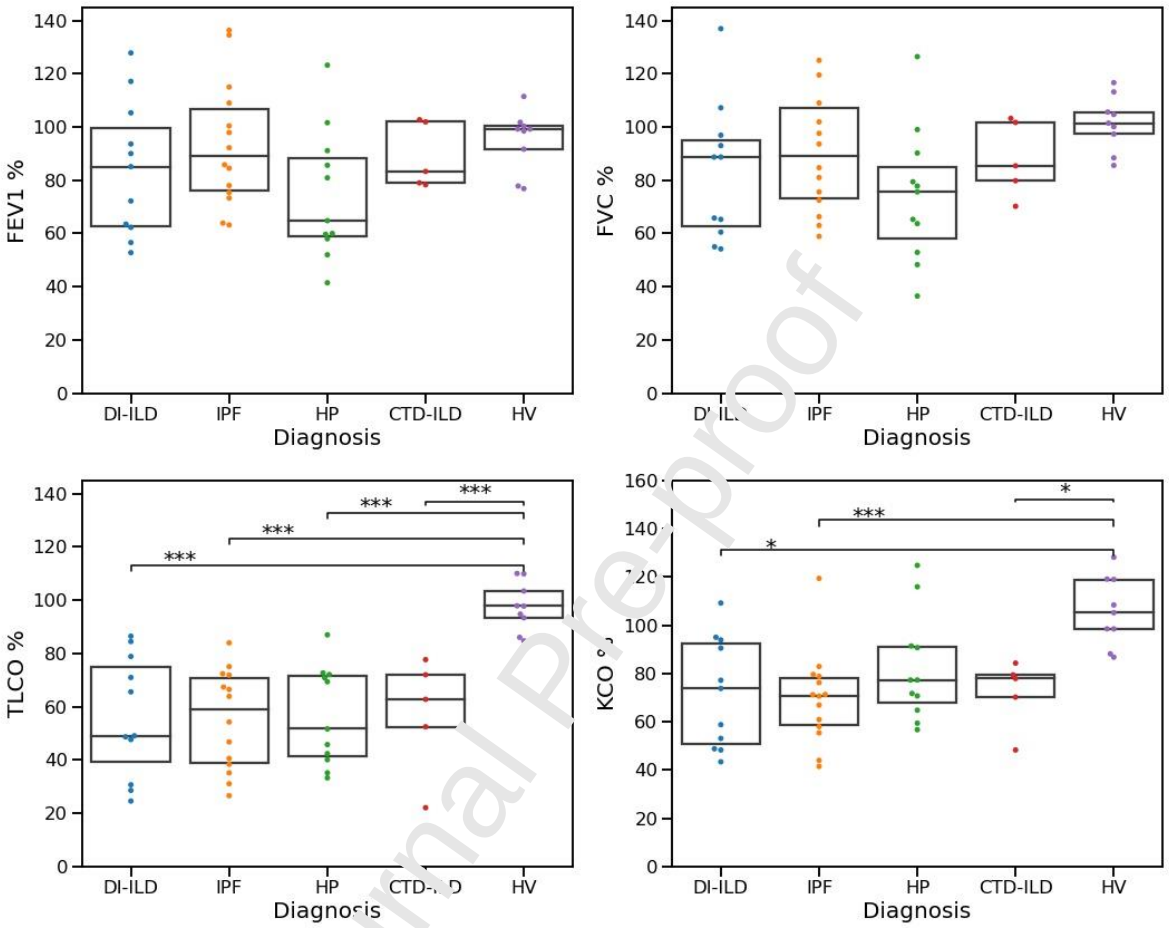

Figure 6: boxplot of pulmonary ^{129}Xe biomarkers at visit 1 in the studied population, split in ILD subgroups. (*) p<0.05, (**) p<0.01, (***) p<0.001. % ^{129}Xe-VVF: percentage of ventilated volume as calculated by ^{129}Xe MRI, Xe-VH_I: ventilation heterogeneity index as calculated by ^{129}Xe

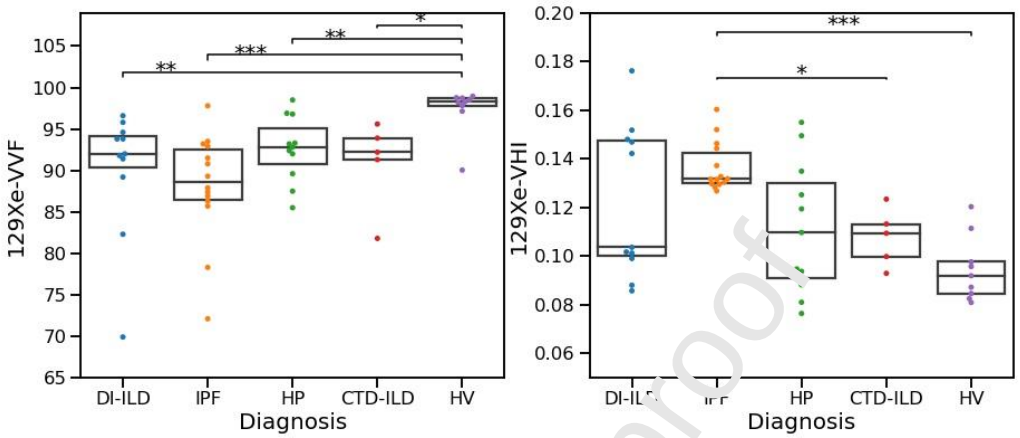

Figure 7: boxplot of pulmonary proton MR biomarkers at visit 1 in the studied population, split in ILD subgroups. (*) p<0.05, (**) p<0.01. ΔpO_2: change in oxygen partial pressure, $\tau_{up:}$ wash-in rate of oxygen, OE-VVF: ventilated volume as calculated by oxygen-enhanced MRI, OE-VH_I: ventilation heterogeneity index as calculated by oxygen-enhanced MRI, T_1: inversion recovery T_1.

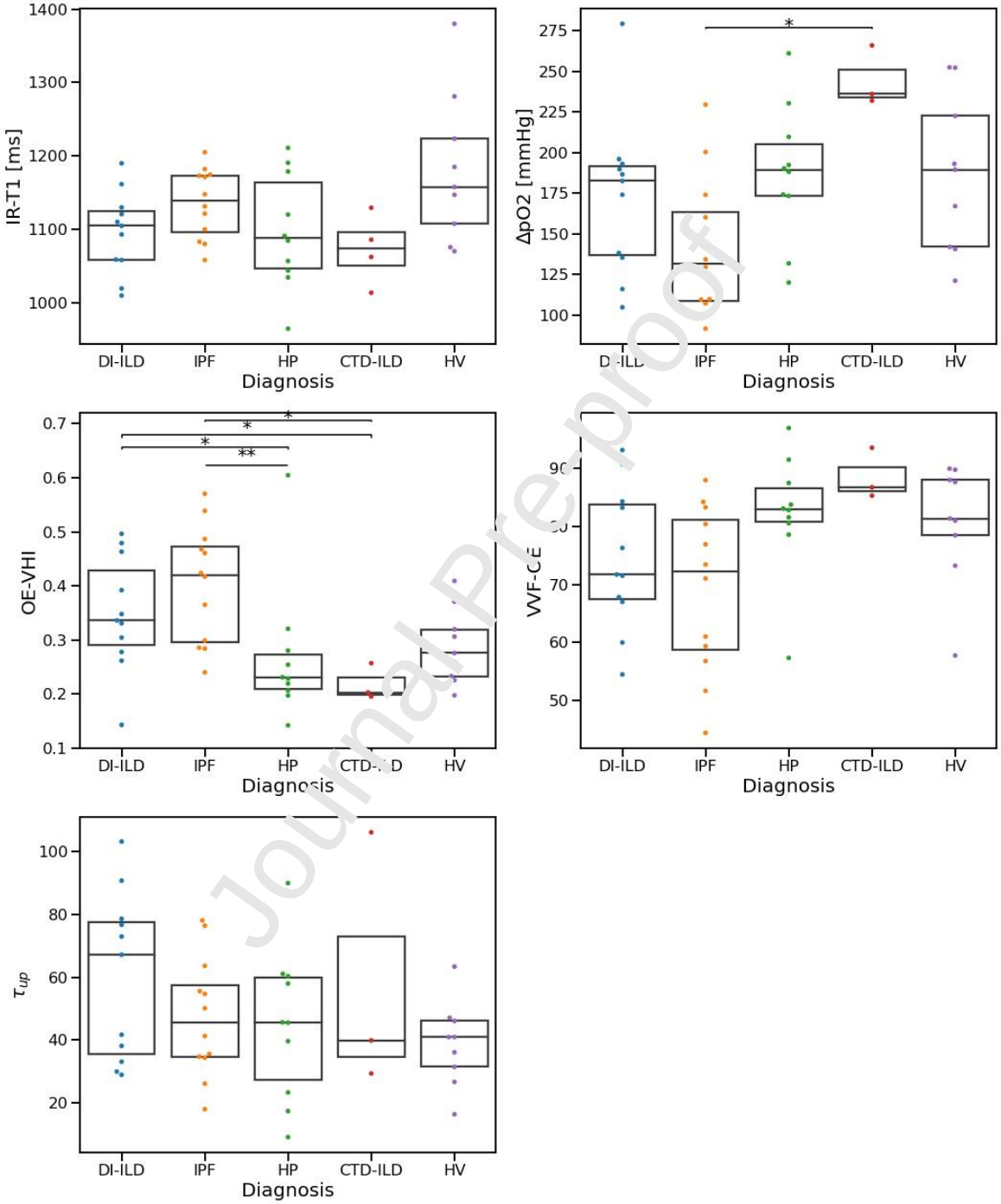

Marta Tibiletti: Software, Visualization, Formal analysis, Writing - Original Draft , Writing - Review & Editing
James A Eaden: Investigation, Data Curation, Writing - Review & Editing
Jo Naish: Software, Supervision, Writing - Review & Editing
Paul JC Hughes: Software, Validation, Visualization, Writing - Review & Editing
John C Waterton: Funding acquisition, Conceptualization, Writing - Review & Editing
Matthew J Heaton: Software, Validation, Data Curation, Writing - Review & Editing
Nazia Chaudhuri: Investigation, Writing - Review & Editing
Sarah Skeoch: Conceptualization, Methodology, Investigation, Writing - Review & Editing
Ian N Bruce: Conceptualization, Methodology, Writing - Review & Editing
Stephen Bianchi: Conceptualization, Methodology, Investigation, Writing - Review & Editing
Jim M Wild: Funding acquisition, Supervision, Writing - Review & Editing
Geoff JM Parker: Funding acquisition, Supervision, Writing - Review & Editing